Available online at www.sciencedirect.com
ScienceDirect
Journal of Organometallic Chemistry 692 (2007) 3248–3260
Journal of Organometallic Chemistry
www.elsevier.com/locate/jorganchem

Half-sandwich η^6-benzene Ru(II) complexes of phenolate-based pyridylalkylamine/alkylamine ligands: Synthesis, structure, and stabilization of one-electron oxidized species

Haritosh Mishra, Rabindranath Mukherjee *

Department of Chemistry, Indian Institute of Technology Kanpur, Kanpur 208 016, India

Received 2 January 2007; received in revised form 21 March 2007; accepted 21 March 2007
Available online 5 April 2007

Abstract

Four half-sandwich ruthenium(II) complexes $[(\eta^6\text{-}C_6H_6)Ru(L^1\text{-}O)][PF_6]$ (**1**), $[(\eta^6\text{-}C_6H_6)Ru(L^2\text{-}O)][PF_6]$ (**2**), $[(\eta^6\text{-}C_6H_6)Ru(L^3\text{-}O)][PF_6]$ (**3**), $[(\eta^6\text{-}C_6H_6)Ru(L^4\text{-}O)][PF_6]$ (**4a**), and $[(\eta^6\text{-}C_6H_6)Ru(L^4\text{-}O)][BPh_4]$ (**4b**) [L^1-OH, 4-nitro-6-{[(2′-(pyridin-2-yl)ethyl)methylamino]methyl}-phenol; L^2-OH, 2,4-di-*tert*-butyl-6-{[(2′-(pyridin-2-yl)ethyl)methylamino]methyl}-phenol; L^3-OH, 2,4-di-*tert*-butyl-6-{[2′-((pyridin-2-yl)benzylamino)methyl}-phenol; L^4-OH, 2,4-di-*tert*-butyl-6-{[(2′-imethylaminoethyl)methylamino]methyl}-phenol (L^4-OH)], supported by a systematically varied series of tridentate phenolate-based pyridylalkylamine and alkylamine ligands are reported. The molecular structures of **1**–**3**, **4a**, and **4b** have been elucidated in solution using ^{1}H NMR spectroscopy and of **1**, **3**, and **4b** in the solid state by X-ray crystallography. Notably, due to coordination by the ligands the Ru center assumes a chiral center and in turn the central amine nitrogen also becomes chiral. The ^{1}H NMR spectra exhibit only one set of signals, suggesting that the reaction is completely diastereoselective [**1**: S_{Ru},S_N/R_{Ru},R_N; **2**: R_{Ru},R_N/S_{Ru},S_N; **3**: S_{Ru},R_N/R_{Ru},S_N; **4b**: S_{Ru},R_N/R_{Ru},S_N]. The crystal packing in **1** and **3** is stabilized by C–H···O interactions, in **4b** no meaningful secondary interactions are observed. From the standpoint of generating phenoxyl radical, as investigated by cyclic voltammetry (CV), complex **1** is redox-inactive in MeCN solution. However, **2**, **3**, and **4a** generate a one-electron oxidized phenoxyl radical coordinated species $[\mathbf{2}]^{2+\cdot}$, $[\mathbf{3}]^{2+\cdot}$, and $[\mathbf{4a}]^{2+\cdot}$, respectively. The radical species are characterized by CV, UV–Vis, and EPR spectroscopy. The stability of the radical species has been determined by measuring the decay constant (UV–Vis spectroscopy).

Keywords: Ruthenum(II); Benzene; Phenolate-based pyridylalkylamine/alkylamine ligands; Diastereoselective; Crystal structures; Non-covalent interactions; Electrochemical oxidation; Phenoxyl radical species

1. Introduction

Half-sandwich η^6-benzene–Ru^{II} complexes belong to a well-established family of metal–organic molecules in organometallic chemistry [1]. The impetus for the synthesis and properties of new complexes having $\{(\eta^6\text{-}C_6H_6)Ru\}^{2+}$ unit arises, owing to their catalytic potential in a range of organic transformations [2] and very promising cytotoxic properties [3]. The present work stems from our continued interest in the synthesis and structural characterization of complexes of types $[(\eta^6\text{-}C_6H_6)Ru(L)]^{2+}$ [4] and $[(\eta^6\text{-}C_6H_6)\text{-}Ru(L')Cl]^{+}$ [5] (L = neutral tridentate pyridylalkylamine ligand; L′ = neutral bidentate heterocyclic pyridyl/pyrazole/imidazole-hybrid N-donor ligands). The purpose of the present study is two-fold. First, although few examples of structurally characterized mononuclear three-legged half-sandwich arene–ruthenium (arene = *p*-cymene) complexes supported by phenol-based Schiff base ligands are known [6], to our knowledge, there is only one report in the literature of a structurally characterized complex [(η^6-*p*-cymene)Ru(L″)Cl] with a non-Schiff base ligand (L″ = bidentate uninegative ligand) [2d]. We are not aware

* Corresponding author. Tel.:/fax: +91 512 2597437/7436.
E-mail address: rnm@iitk.ac.in (R. Mukherjee).

0022-328X/$ - see front matter © 2007 Elsevier B.V. All rights reserved.
doi:10.1016/j.jorganchem.2007.03.041

of any structurally characterized arene–ruthenium complex of tridentate uninegative non-Schiff base phenol/pyridylalkylamine/alkylamine-hybrid chelating ligand. From the standpoint of synthetic chemistry we find it really challenging. To provide such examples in this study we have utilized simple but systematically modified tridentate ligands (L^1-OH, L^2-OH, L^3-OH, and L^4-OH; Scheme 1), in their deprotonated form. As before [5] we wished to test if the different electronic/steric environment provided by a particular tridentate ligand has an impact on the relative strength of the Ru–benzene bonding in these three-legged "piano-stool" $\{(\eta^6\text{-}C_6H_6)Ru(L)\}^+$ complexes. Secondly, due to covalency in a bond elementary chemical reactions in general and catalysis in particular mostly involve two-electron changes in the metal coordination sphere. However, one-electron processes are also of fundamental importance in organometallic chemistry [7]. Notably, a long-standing problem in the redox chemistry of metal–organic molecules of ligands that are themselves potential sites of facile electron transfer is identifying whether the site of redox is metal-centered or ligand-centered [8]. From this standpoint we have initiated a program to synthesize half-sandwich complexes with redox-active ligands. Among the ligands chosen in this work (Scheme 1), the ligands L^2-OH, L^3-OH, and L^4-OH contain 2,4-di-*tert*-butyl-phenolate groups and are redox-active [9]. Studies on redox chemistry followed by spectral characterization (absorption and EPR) of one-electron oxidized (ligand-centered oxidation) counterparts of original ligands is expected to provide information pertinent to understanding of the stability/reactivity of such metal-coordinated radical species. Our present endeavor in this area is set against this background.

2. Experimental

2.1. Materials

Reagent or analytical grade starting materials were obtained from commercial suppliers and used without further purification. 2,4-di-*tert*-butyl-6-(hydroxymethyl)- phenol [9a] and 2,4-di-*tert*-butyl-6-(chloromethyl)phenol [9h] were synthesized following the literature procedures. The ligand 2,4-di-*tert*-butyl-6-{[(2′-dimethylaminoethyl)methylamino]methyl}-phenol (L^4-OH) [10] and the dimer $[\{(\eta^6\text{-}C_6H_6)RuCl(\mu\text{-}Cl)\}_2]$ [11] were prepared following literature methods.

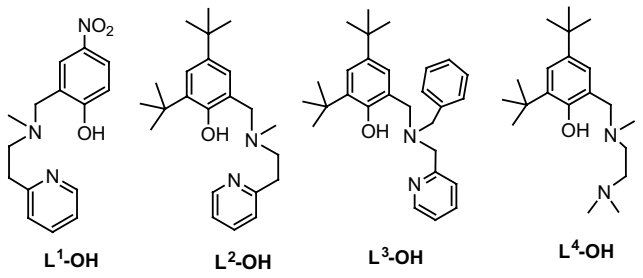

Scheme 1.

2.2. Preparation of ligand

2.2.1. 4-Nitro-6-{[(2′-(pyridin-2- yl)ethyl)methylamino]-methyl}-phenol (L^1-OH)

A mixture of *N*-methyl-2-(pyridin-2-yl)ethanamine (1.09 g, 8.00 mmol) and triethylamine (0.81 g, 8.00 mmol) in CH_3OH (20 mL) was stirred at 25 °C to which was added a solution of 2-(chloromethyl)-4-nitrophenol (1.50 g, 8.00 mmol) in CH_3OH (20 mL) dropwise over a period of 30 min under nitrogen atmosphere. The resulting mixture was refluxed for 2.5 h and then cooled to room temperature. The solvent was evaporated under reduced pressure and the yellow sticky solid that obtained was dissolved in dry THF (20 mL) and cooled to 0 °C. Triethylammonium chloride that precipitated was filtered off and the filtrate was evaporated to dryness under reduced pressure to give 2 g of crude product. The yellow sticky crude oil was subjected to column chromatography on silica gel by using CH_2Cl_2 as eluent. Solvent was removed to yield yellow sticky oil which solidified after recrystallization from CH_2Cl_2/*n*-hexane. Yield: 1.60 g (70%). ^{1}H NMR (80 MHz; $CDCl_3$): δ 8.63 (d, 1H, H_6 of py), 8.50–6.8 (m, 6H, $H_{3,4,5}$ of py and $H_{3,5,6,}$ of PhOH), 4.82 (s, 2H, –CH_2– of PhOH), 3.50–3.10 (s, 4H, –CH_2CH_2– of Py), 2.40 (s, 3H, –CH_3).

2.2.2. 2,4-Di-tert-butyl-6-{[(2′-(pyridin-2- yl)ethyl)-methylamino]methyl}-phenol (L^2-OH)

Triethylamine (1.3 mL) was added dropwise to a stirring mixture of *N*-methyl-2-(pyridin-2-yl)ethanamine (0.272 g, 2 mmol) and 2,4-di-*tert*-butyl-6-(chloromethyl)-phenol (0.509 g, 2 mmol) in dry dioxane (3 mL). After stirring the mixture for 2 h it was heated to 60 °C and more triethylamine (2 mL) was added dropwise over a period of 2 h. During this addition of triethylamine, the pH of the mixture was maintained below 10. The reaction mixture was then cooled to room temperature, further stirred for 15 min, and filtered. Solvent and excess of triethylamine was removed under reduced pressure to obtain the product as yellow sticky oil. Yield: 0.500 g, ca. 71%. ^{1}H NMR (80 MHz; $CDCl_3$): δ 8.33 (d, 1H, H_6 of py), 7.45–6.46 (m, 5 H, $H_{3,4,5}$ of py and $H_{3,5,}$ of PhOH), 3.66 (s, 2H, –CH_2– of PhOH), 2.90 (s, 4H, –CH_2CH_2– of Py), 2.15 (s, 3H, –NCH_3), 1.33 (s, 9H, *2*-*tert*-butyl), 1.15 (s, 9H, *4*-*tert*-butyl).

2.2.3. 2,4-Di-tert-butyl-6-{[2′-((pyridin-2-yl)benzylamino)methyl}-phenol (L^3-OH)

The starting material phenyl-*N*-(pyridin-2-ylmethyl)-methanamine necessary for the synthesis of L^3-OH was prepared by the following procedure. A solution of pyridin-2-ylmethanamine (0.540 g, 5 mmol) and benzaldehyde (0.530 g, 5 mmol) in C_2H_5OH (10 mL) was stirred for 1 h at 25 °C, under dinitrogen atmosphere. Solid $NaBH_4$ (0.760 g, 10 mmol) was then added slowly in small portions

over a period of 30 min and the resulting suspension was further stirred at 25 °C for 30 min, under dinitrogen atmosphere. The reaction mixture was then refluxed for 12 h. After cooling to 25 °C, the mixture was diluted with C_2H_5OH (10 mL) and excess of $NaBH_4$ was destroyed by adding aq. HCl (10 mL, 5 M) dropwise. The reaction mixture was then made alkaline by 20% aq. NaOH solution (pH 12). Finally, the desired product was extracted in CH_2Cl_2 (4×10 mL) and dried over anhydrous $MgSO_4$. The solvent was evaporated under reduced pressure to get yellow oil. The oil was then dried *in vacuo* and used in the next step, without further purification. Yield: 0.750 g, ca. 75%. ^{1}H NMR (80 MHz; $CDCl_3$): δ 8.30 (d, 1H, H_6 of py), 7.33–6.66 (m, 8H, $H_{3,4,5}$ of py and H_{2-6} of Ph), 3.45 (s, 4H, $-CH_2-$).

In the next step, phenyl-*N*-(pyridin-2-ylmethyl)methanamine (0.396 g, 2 mmol) and 2,4-di-*tert*-butyl-6-(chloromethyl)-phenol (0.509 g, 2 mmol) were coupled following the above-mentioned method for the synthesis of ligand L^2-OH. Yield: 0.530 g, ca. 63%. ^{1}H NMR (80 MHz; $CDCl_3$): δ 8.40 (d, 1H, H_6 of py), 7.25–6.45 (m, 10H, $H_{3,4,5}$ of py, H_{2-6} of Ph and $H_{3,5,}$ of PhOH), 3.25 (s, 2H, $-CH_2-$ of PhOH), 3.15 (4H, s, $-CH_2-$ of Ph and $-CH_2-$ of Py), 1.46 (s, 9H, *2-tert*-butyl), 1.15 (s, 9H, *4-tert*-butyl).

2.3. Preparation of complexes

2.3.1. General procedure

A mixture of the ligand (0.4 mmol) and triethylamine (0.4 mmol) was dissolved in CH_3OH (15 mL) under dinitrogen atmosphere and to it was added solid [{(η^6-C_6H_6)RuCl(μ-Cl)}$_2$] (0.2 mmol). The mixture was stirred for 8 h (complexes **1** and **3**) or 12 h (complexes **2** and **4a**) at 25 °C. The resulting reddish yellow (complexes **1** and **3**) or reddish orange (complexes **2** and **4a**) solution was filtered and the volume of the filtrate was reduced (~5 mL) and to it was added solid NH_4PF_6 (0.4 mmol). For complex **3** the resulting mixture was heated at 65 °C for 10 min and cooled to 25 °C. The yellow (complex **2**) or orange (complexes **3** and **4a**) microcrystalline solid that formed was filtered, washed with cold CH_3OH, and dried in vacuo. The complex **1** was precipitated out by addition of diethyl ether (10 mL) into the filtrate which led to isolation of an orange solid. It was filtered, washed with a mixture of diethyl ether and CH_3OH (2:1; v/v), and dried *in vacuo*. Recrystallization was achieved from CH_3CN/diethyl ether (**1**, **3**, and **4a**) or from CH_3CN and CH_3OH (1:1; v/v)/diethyl ether (**2**). X-ray quality single-crystals were obtained by diffusion of diethyl ether into a solution (1 mL) of the compound in MeCN (complex **1**) or in a mixture (v/v; 3:1) of CH_3OH and CH_3CN (complex **3**).

2.3.2. [(η^6-C_6H_6)Ru(L^1-O)][PF_6] (**1**)

Yield: 0.140 g (57%). Anal. Calc. for $C_{21}H_{22}N_3F_6O_3PRu$: C, 41.31; H, 3.60; N, 6.88. Found: C, 41.29; H, 3.52; N, 6.91%. IR (KBr, cm^{-1}): 1518 $\nu_{asym}(NO_2)$, 1330 $\nu_{sym}(NO_2)$, 842 ν (PF_6^-). ^{1}H NMR (CD_3CN; 400 MHz; 298 K): δ 8.95 (d, $J_{HH} = 5.6$ Hz, 1H, H_6 of py), 7.85–7.77 (m, 2H, H_4 of py and $H_{6'}$ of PhO), 7.67 (d, $J_{HH} = 7.0$ Hz, 1H, $H_{5'}$ of PhO), 7.40 (s, 1H, $H_{3'}$ of PhO), 7.36 (t, $J_{HH} = 7.8$ Hz, 1H, H_5 of py), 6.68 (d, $J_{HH} = 9.0$ Hz, 1H, H_3 of py) 5.80 (s, 6H, C_6H_6), 3.89 (d, $J_{gem} = 12.7$ Hz, 1H, $-CH_2-$), 3.66 (s, 3H, $-NCH_3$), 3.20 (m, 1H, $-CH_2CH_2-$), 3.07 (m, 1H, $-CH_2CH_2-$), 2.99 (d, $J_{gem} = 12.7$ Hz, 1H, $-CH_2-$), 2.55 (m, 1H, $-CH_2-CH_2-$), 2.01 (m, 1H, $-CH_2CH_2-$). Molar conductance, Λ_M(CH_3CN, 298 K) = 125 Ω^{-1} cm^2 mol^{-1} (expected 1:1 range: 120–160 Ω^{-1} cm^2 mol^{-1}). UV–Vis (in CH_3CN): λ/nm (ε/dm^3 mol^{-1} cm^{-1}) 380 (19 100), 270 sh (7500), 235 sh (15 400).

2.3.3. [(η^6-C_6H_6)Ru(L^2-O)][PF_6] (**2**)

Yield: 0.170 g (63%). Anal. Calc. for $C_{29}H_{39}N_2F_6OPRu$: C, 51.40; H, 5.76; N, 4.13. Found: C, 50.79; H, 5.80; N, 4.18%. IR (KBr, cm^{-1}): 2951 ν(C–H of *tert*-butyl), 840 $\nu(PF_6^-)$. ^{1}H NMR (CD_3CN; 400 MHz; 298 K): δ 8.98 (d, $J_{HH} = 4.8$ Hz, 1H, $H_{6'}$ of py), 7.46 (t, $J_{HH} = 7.56$ Hz, 1H, $H_{4'}$ of py), 7.48 (d, $J_{HH} = 7.8$ Hz, 1H, $H_{3'}$ of py), 7.36 (t, $J_{HH} = 6.2$ Hz, 1H, $H_{5'}$ of py), 7.10 (d, $J^{1\text{-}4}_{HH} = 2.6$ Hz, 1H, H_3 of PhO), 6.56 (d, $J^{1\text{-}4}_{HH} = 2.6$ Hz, 1H, H_5 of PhO), 5.84 (s, 6H, C_6H_6), 3.41 (m, 1H, $-CH_2CH_2-$), 3.31 (m, 1H, $-CH_2CH_2-$, overlaped with $-NCH_3$), 3.29 (s, 3H, $-NCH_3$), 2.77 (d, $J_{gem} = 12.7$ Hz, 1 H $-CH_2-$), 2.73 (m, 1H, $-CH_2CH_2-$), 1.98 (d, $J_{gem} = 12.7$ Hz, 1H $-CH_2-$) 1.53 (s, 9H, *o-tert*-butyl), 1.15 (s, 9H, *p-tert*-butyl). Molar conductance, Λ_M(CH_3CN, 298 K) = 110 Ω^{-1} cm^2 mol^{-1}. UV–Vis (in CH_3CN): λ/nm (ε/dm^3 mol^{-1} cm^{-1}) 450 sh (1000), 350 sh (2450), 305 sh (8100), 254 (24 500).

2.3.4. [(η^6-C_6H_6)Ru(L^3-O)][PF_6] (**3**)

Yield: 0.150 g (50%). Anal. Calc. for $C_{34}H_{41}N_2F_6OPRu$: C, 55.20; H, 5.54; N, 3.78. Found: C, 54.98; H, 5.53; N, 3.81%. IR (KBr, cm^{-1}): 2950 ν(C–H of *tert*-butyl), 838 $\nu(PF_6^-)$. ^{1}H NMR (CD_3CN; 400 MHz; 298 K): δ 8.75(d, $J_{HH} = 5.8$ Hz, 1H, $H_{6'}$ of py), 7.66–7.54 (d m, 5H, phenyl), 7.44 (t, $J_{HH} = 8.4$ Hz, 1H, $H_{4'}$ of py), 6.95 (t, $J_{HH} = 6.5$ Hz, 1 H, $H_{5'}$ of py), 6.84 (d, $J_{HH} = 7.8$ Hz, 1H, $H_{3'}$ of py), 6.69 (d, $J^{1\text{-}4}_{HH} = 2.4$ Hz, 1H, H_3 of PhO), 6.14 (d, $J^{1\text{-}4}_{HH} = 2.4$ Hz, 1H, H_5 of PhO), 5.94 (s, 6H, C_6H_6), 5.45 (dd, 2H, $J_{gem} = 12.9$ Hz, $H_{a''}$ and $H_{b''}$ of $-CH_2-$ of pyridyl), 4.72 (d, $J_{gem} = 15.3$ Hz, 1H, $H_{a'}$ of $-CH_2-$ of PhO), 3.83 (d, $J_{gem} = 15.3$ Hz, 1H, $H_{b'}$ of $-CH_2-$ of PhO), 3.39 (d, $J_{gem} = 11.2$ Hz, 1H, H_b of $-CH_2-$ of Benzyl), 2.98 (d, $J_{gem} = 11.2$ Hz, 1H, H_a of $-CH_2-$ of Benzyl), 1.37 (s, 9H, *o-tert*-butyl), 0.94 (s, 9H, *p-tert*-butyl). Molar conductance, Λ_M(CH_3CN, 298 K) = 120 Ω^{-1} cm^2 mol^{-1}. UV–Vis (in CH_3CN): λ/nm (ε/dm^3 mol^{-1} cm^{-1}) 430 sh (1550), 325 sh (5700), 270 sh (10 200), 250 sh (17 600).

2.3.5. [(η^6-C_6H_6)Ru(L^4-O)][PF_6] (**4a**)

Yield: 0.165 g (64%). Anal. Calc. for $C_{26}H_{41}N_2F_6OPRu$: C, 48.52; H, 6.37; N, 4.35. Found: C, 48.54; H, 6.37; N, 4.37%. IR (KBr, cm^{-1}): 2951 ν(C–H of *tert*-butyl), 839 $\nu(PF_6^-)$. ^{1}H NMR (CD_3CN; 400 MHz; 298 K): δ 7.14 (d, $J^{1\text{-}4}_{HH} = 2.6$ Hz, 1 H, H_3 of PhO), 6.74 (d, $J^{1\text{-}4}_{HH} = 2.6$ Hz,

1H, H_5 of PhO), 5.65 (s, 6H, C_6H_6), 4.68 (d, 1H, $J_{gem} = 14.9$ Hz, –CH_2–), 3.53 (s, 3H, -N(CH_3)$_2$), 3.48 (d, 1H, $J_{gem} = 14.9$ Hz, –CH_2–), 3.41 (m, 1H, –CH_2CH_2–), 3.37 (s, 3H, –N(CH_3)$_2$), 2.69 (s, 3H, –NCH_3), 2.57 (m, 1H, –CH_2CH_2–), 2.43 (m, 1H, –CH_2CH_2–), 2.16 (m, 1H, –CH_2CH_2–, overlaped with H_2O signal), 1.45 (s, 9H, *2-tert*-butyl), 1.22 (s, 9H, *6-tert*-butyl). Molar conductance, Λ_M(CH_3CN, 298 K) = 120 Ω^{-1} cm^2 mol^{-1}. UV–Vis (in CH_3CN): λ/nm (ε/dm^3 mol^{-1} cm^{-1}) 460 sh (700), 306 (6800), 253 (19 500).

2.3.6. [(η^6-C_6H_6)Ru(L^4-O)][BPh_4] (**4b**)

Compound **4a** (0.064 g, 0.1 mmol) was dissolved in CH_3CN (2 mL) and to it was added a solution of $NaBPh_4$ (0.040 g, 0.116 mmol) in CH_3OH (4 mL) dropwise. The resulting mixture was stirred for 10 min at 25 °C and the orange solution was filtered through celite pad. Diffusion of diethyl ether into the filtrate yielded an orange microcrystalline solid, which was filtered, washed with CH_3OH, and dried *in vacuo*. X-ray quality single-crystals were obtained by diffusion of diethyl ether into a solution (1 mL) of the compound in a mixture (v/v; 3:1) of CH_3OH and CH_3CN. Yield: 0.075 g (90%). Anal. Calc. for $C_{50}H_{61}N_2BORu$: C, 73.43; H, 7.46; N, 3.42. Found: C, 73.44; H, 7.45; N, 3.44%. ^{1}H NMR (CD_3CN; 400 MHz; 298 K): δ 7.26 (m, 8H, $H_{2',6'}$ of BPh_4^-), 7.14 (d, $J^{1-4}_{HH} = 2.4$ Hz, 1H, H_3 of PhO), δ 6.98 (t, 8H, $J_{HH} = 7.5$ Hz, $H_{3',5'}$ of BPh_4^-), 6.83 (t, 4H, $J_{HH} = 7.0$ Hz, $H_{4'}$ of BPh_4^-), 6.73 (d, $J^{1-4}_{HH} = 2.4$ Hz, 1H, H_5 of PhO), 5.61 (s, 6H, C_6H_6), 4.65 (d, 1H, $J_{gem} = 14.4$ Hz, –CH_2–), 3.49 (s, 3H, –N(CH_3)$_2$), 3.45 (d, 1H, $J_{gem} = 14.4$ Hz, –CH_2–), 3.41 (m, 1H, –CH_2CH_2–), 3.33 (s, 3H, –N(CH_3)$_2$), 2.67 (s, 3H, –NCH_3), 2.55 (m, 1H, –CH_2CH_2–), 2.43 (m, 1H, –CH_2CH_2–), 2.16 (m, 1H, –CH_2CH_2–, overlaped with H_2O signal), 1.44 (s, 9H, *o-tert*-butyl), 1.21 (s, 9H, *p-tert*-butyl). Molar conductance, Λ_M(CH_3CN, 298 K) = 80 Ω^{-1} cm^2 mol^{-1}. UV–Vis (in CH_3CN): λ/nm (ε/dm^3 mol^{-1} cm^{-1}) 460 sh (750), 305 (6500), 253 (21 500).

2.4. Instrumentation

Elemental analyses were obtained using Thermo Quest EA 1110 CHNS-O, Italy. Conductivity measurements were done with an Elico type CM-82T conductivity bridge (Hyderabad, India). Spectroscopic measurements were made using the following instruments: IR (KBr, 4000–600 cm^{-1}), Bruker Vector 22; electronic, Perkin–Elmer Lambda 2 and Agilent 8453 diode-array spectrophotometer. ^{1}H NMR spectral measurements were performed on a JEOL-JNM-LA-400 FT (400 MHz) NMR spectrometer. X-band EPR, Bruker EMX 1444 spectrometer operating at 9.455 GHz. The EPR spectra were calibrated with diphenylpicrylhydrazyl, DPPH ($g = 2.0037$).

The cyclic voltammetric experiments were performed at 298 K by using a CH Instruments, Electrochemical Analyzer/Workstation Model 600B Series. A standard three electrode cell was employed with a Beckman M-39273 platinum-inlay working electrode, a platinum-wire auxiliary electrode and a saturated calomel electrode (SCE) as reference; no corrections were made for junction potentials. Details of cell configuration and criterion for reversibility are as reported previously [8]. For constant potential electrolysis experiments a Pt mesh was used as working electrode. The solutions were ~1 mM in complexes and 0.1 M in supporting electrolyte, TBAP. Under our experimental conditions, in CH_3CN the $E_{1/2}$ value (V) for F_c^+/F_c couple was 0.40 vs. SCE [8].

2.5. Crystal structure determination

Diffracted intensities were collected on a Bruker SMART APEX CCD diffractometer at 100(2) K (**1**), (**3**), and (**4b**) · 1/2CH_3OH · H_2O 293(2) K using graphite monochromated Mo Kα ($\lambda = 0.710\ 69$ Å) radiation. Intensity data were corrected for Lorentz polarization effects. Empirical absorption correction (SADABS) was applied. The structures were solved by SIR-97, expanded by Fourier-difference syntheses and refined with SHELXL-97, incorporated in WinGX 1.64 crystallographic collective package [12]. Hydrogen atoms were placed in idealized positions, and treated using riding model approximation with displacement parameters derived from those of the atoms to which they were bonded. All non-hydrogen atoms were refined with anisotropic thermal parameters by full-matrix least-squares procedures on F^2. For **4b** · 1/2CH_3OH · H_2O, some degree of disorder was observed with H_2O molecule; two positions for O2W atom could be located and they were refined with a site occupation factor of 0.6/0.4. A summary of the data collection and structure refinement information is provided in Table 1. For complex **4b** · 1/2CH_3OH · H_2O, after anisotropic refinement some unassigned electron density peaks were observed in the final difference Fourier map. For **4b** · 1/2CH_3OH · H_2O peaks of 5.50 e Å^{-3} and 4.01 e Å^{-3} were found near Ru1′ and Ru1 atom at a distance of 1.310 Å and 1.254 Å, respectively, which may be due to the poor quality of crystal chosen for data collection (high R_{int} value). Unfortunately, we could not grow single crystals of **4a**/**4b** that were any better than the one used for the present study, as they were the best we could have. The overall crystal refinement was poor (Table 1). A preliminary structural drawing of compound **2** has been presented in the Supplementary data for its authenticity (the details of which will be published elsewhere). Intermolecular contacts of the C–H···O type were examined with the DIAMOND package [13]. C–H distances were normalized along the same vectors to the neutron derived values of 1.083 Å [14].

3. Results and discussion

3.1. Synthesis and characterization of complexes

From the standpoint of bridge-cleavage reactivity of chloro-bridged dimer [{(η^6-C_6H_6)RuCl(μ-Cl)}$_2$] reactions

Table 1
Data collection and structure refinement parameters for $[(\eta^6\text{-}C_6H_6)Ru(L^1\text{-}O)][PF_6]$ (**1**), $[(\eta^6\text{-}C_6H_6)Ru(L^3\text{-}O)][PF_6]$ (**3**), and $[(\eta^6\text{-}C_6H_6)Ru(L^4\text{-}O)][BPh_4]\cdot 1/2CH_3OH\cdot H_2O$ (**4b** $\cdot 1/2CH_3OH\cdot H_2O$)

	1	**3**	**4b** $\cdot 1/2CH_3OH\cdot H_2O$
Chemical formula	$C_{21}H_{22}N_3O_3\text{-}PF_6Ru$	$C_{34}H_{41}N_2O\text{-}PF_6Ru$	$C_{50.5}H_{62}N_2O_{2.5}\text{-}BRu$
M	610.46	504.76	849.41
Crystal color, habit	Orange, block	Orange, block	Orange, block
T (K)	100(2)	293(2)	293(2)
Crystal system	Triclinic	Triclinic	Triclinic
Space group	$P\bar{1}$ (#2)	$P\bar{1}$ (#2)	$P\bar{1}$ (#2)
a (Å)	7.7629(11)	9.7737(16)	13.431(5)
b (Å)	9.8439(13)	11.8689(19)	19.070(5)
c (Å)	14.995(2)	15.843(3)	19.801(5)
α (°)	98.883(2)	109.348(2)	111.006(5)
β (°)	98.249(2)	102.390(3)	90.162(5)
γ (°)	103.616(2)	97.006(3)	99.539(5)
V (Å^3)	1080.8(3)	1656.1(5)	4658(2)
Z	2	2	4
d_{calc} (g cm^{-3})	1.876	1.483	1.211
μ (mm^{-1})	0.883	0.585	0.377
$F(000)$	612	760	1794
Number of reflections collected	7224	11 047	31 343
Number of independent reflections [R (int)]	5110 [0.0307]	7905 [0.0210]	22 286 [0.0609]
Number of reflections used [$I > 2\sigma(I)$]	4305	6505	10530
Goodness-of-fit on F^2	1.170	1.026	0.986
Final R indices [$I > 2\sigma(I)$][a,b]	0.0574, 0.1206	0.0525, 0.1276	0.1152, 0.2944
Final R indices (all data)	0.0759, 0.1527	0.0748, 0.1808	0.2103, 0.3482

[a] $R_1 = \sum(|F_o| - |F_c|)/\sum|F_o|$.
[b] $wR_2 = \{\sum[w(|F_o|^2 - |F_c|^2)^2]/\sum[w(|F_o|^2)^2]\}^{1/2}$.

with L^1-OH, L^2-OH, L^3-OH, and L^4-OH (Scheme 1) in CH_3OH in presence of triethylamine followed by subsequent treatment with NH_4PF_6 led to the isolation of $[(\eta^6\text{-}C_6H_6)Ru(L^1\text{-}O)][PF_6]$ (**1**), $[(\eta^6\text{-}C_6H_6)Ru(L^2\text{-}O)][PF_6]$ (**2**), $[(\eta^6\text{-}C_6H_6)Ru(L^3\text{-}O)][PF_6]$ (**3**), and $[(\eta^6\text{-}C_6H_6)Ru(L^4\text{-}O)][PF_6]$ (**4a**) as yellow to yellow–orange microcrystalline solids. It is to be noted here that triethylamine is essential during the course of complex formation for deprotonation of phenolic hydroxyl groups of the chosen ligands to generate anionic ligands $L^1\text{-}O^-$, $L^2\text{-}O^-$, $L^3\text{-}O^-$, and $L^4\text{-}O^-$. The complex $[(\eta^6\text{-}C_6H_6)Ru(L^4\text{-}O)][BPh_4]$ (**4b**) was prepared by simple metathesis reaction between $[(\eta^6\text{-}C_6H_6)Ru(L^4\text{-}O)][PF_6]$ (**4a**) and $NaBPh_4$ in a mixture of CH_3CN and CH_3OH (v/v; 1:2).

Characterization of the new compounds was accomplished by elemental analysis, solution electrical conductivity, IR, and ^{1}H NMR spectroscopy. Consistent with their formulation, IR stretching vibration of PF_6^- at ~840 cm^{-1} confirm cationic nature of complexes **1**–**4a** and conductivity studies revealed that compounds **1**–**3**, **4a**, and **4b** are 1:1 electrolyte [15]. As proof of their color, compounds **1**–**3**, **4a**, and **4b** exhibit absorption spectral band in the 380–460 nm region.

3.2. Molecular structures of $[(\eta^6\text{-}C_6H_6)Ru(L^1\text{-}O)][PF_6]$ (**1**), $[(\eta^6\text{-}C_6H_6)Ru(L^3\text{-}O)][PF_6]$ (**3**), and $[(\eta^6\text{-}C_6H_6)Ru(L^4\text{-}O)][BPh_4]\cdot 1/2CH_3OH\cdot H_2O$ (**4b** $\cdot 1/2CH_3OH\cdot H_2O$)

X-ray crystallographic analyses confirm the structure of the compounds **1**, **3**, and **4b** $\cdot 1/2CH_3OH\cdot H_2O$ (Fig. 1, Table 2). As already mentioned, due to the poor quality of the data set the refinement of the structure of **4b** $\cdot 1/2CH_3OH\cdot H_2O$ (its asymmetric unit contains crystallographically independent two molecules) did not reach a satisfactory level. Nevertheless, the cation seems to have been determined well [Fig. 1c]. The cations exhibit the expected and usual pseudo-octahedral half-sandwich ''piano-stool'' disposition around the Ru atom. The ruthenium(II) ion is π bonded to the $\eta^6\text{-}C_6H_6$ group with the benzene ligand occupying one face of the octahedron and the coordination of a tridentate phenolate-based ligand on the other face [N(1) of pyridine in **1** and **3** or alkylamine in **4b** $\cdot 1/2CH_3OH\cdot H_2O$; N(2) of alkylamine, and O(1) of phenolate]. The pyridyl rings in **1** and **3** and phenolate rings of $L^1\text{-}O^-$ in **1**, of $L^3\text{-}O^-$ in **3**, and of $L^4\text{-}O^-$ in **4b** $\cdot 1/2CH_3OH\cdot H_2O$ are each planar. However, the pyridyl mean plane of **1** and **3** is tilted to the phenolate ring at an angle of 81.754° and 37.895°, respectively.

Interestingly, X-ray structural analyses revealed noticeable differences in the bonding characteristics (metric parameters) of tridentate ligands $L^1\text{-}O^-$, $L^3\text{-}O^-$, and $L^4\text{-}O^-$ as well as the characteristics of π-bonded benzene rings in these cations (Tables 2 and 3). From a careful look at the metric parameters of Table 3, which lists pertinent bonding parameters the following generalizations emerge. (i) The Ru–O(phenolate) bond is strongest in **4b** $\cdot 1/2CH_3OH\cdot H_2O$ [2.041(5) Å {2.040(5) Å}] followed by that in **3** [2.054(3) Å], and weakest in **1** [2.096(4) Å]. It is understandable given the fact that in $L^3\text{-}O^-$ and $L^4\text{-}O^-$, two electron-releasing *tert*-butyl groups are present at the *ortho* and *para* position of the phenolate ring, whereas in $L^1\text{-}O^-$ an

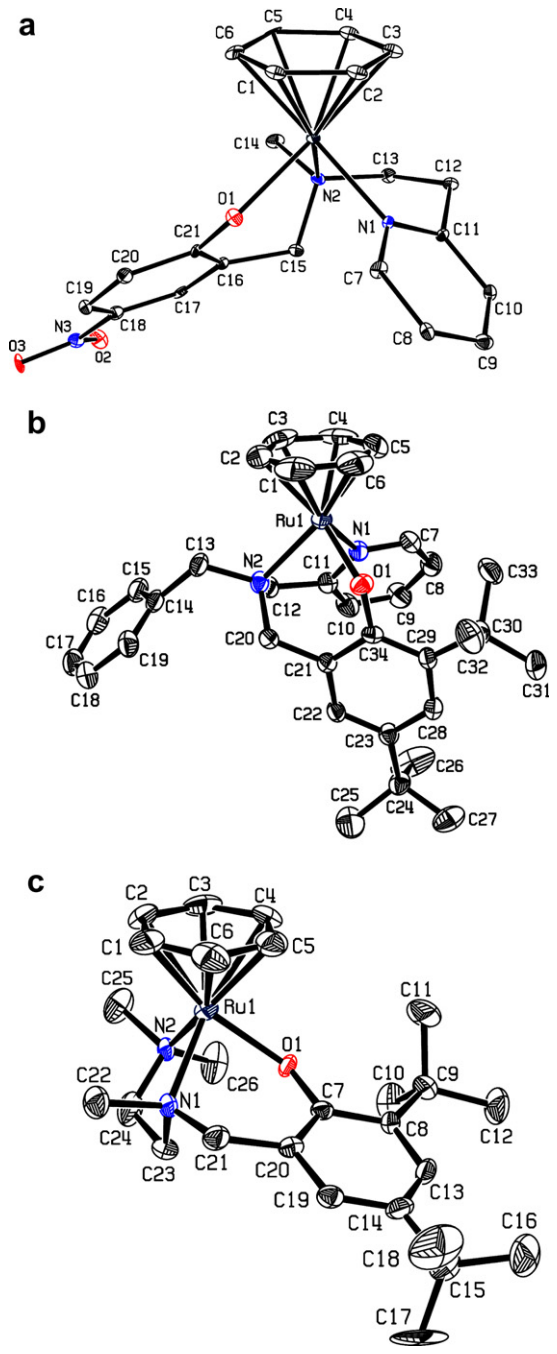

Fig. 1. Thermal ellipsoid plots of (a) (S_{Ru}, S_N)-[(η^6-C_6H_6)Ru(L^1-O)]$^+$ in **1**, (b) (S_{Ru}, R_N)-[(η^6-C_6H_6)Ru(L^3-O)]$^+$ in **3**, and (c) (S_{Ru}, R_N)-[(η^6-C_6H_6)Ru(L^4-O)]$^+$ in (**4b**) · 1/2CH_3OH · H_2O at 30% probability level. Hydrogen atoms have been omitted for clarity.

electron-withdrawing nitro group is present at the *para* position of the phenolate ring. (ii) The Ru–N(py) bond is of equal strength in **1** [2.098(5) Å] and **3** [2.104(4) Å]. The slightly shorter Ru–N(py) bond distance (Table 3) in **1** than in **3** may be attributed to the temperature difference at which the data of the two complexes were collected. (iii) The Ru–N(amine) bond is strongest in **4b** · 1/2CH_3OH · H_2O [2.141(6) {2.147(6)} Å] and weakest in **3** [2.203(4) Å]. This finding reflects the greater inductive effect

Table 2
Selected bond lengths (Å) and angles (°) in [(η^6-C_6H_6)Ru(L^1-O)][PF_6] (**1**), [(η^6-C_6H_6)Ru(L^3-O)][PF_6] (**3**), and [(η^6-C_6H_6)Ru(L^4-O)][BPh_4] · 1/2CH_3OH · H_2O (**4b** · 1/2CH_3OH · H_2O)

	1	**3**	**4b** · 1/2CH_3OH · H_2O
Ru(1)–N(1)	2.098(5)	2.104(4)	2.141(6) [2.147(6)][a]
Ru(1)–N(2)	2.170(5)	2.203(4)	2.1408(8) [2.1443(12)][a]
Ru(1)–O(1)	2.096(4)	2.054(3)	2.041(5) [2.040(5)][a]
Ru(1)–C(1)	2.195(6)	2.180(6)	2.182(10) [2.176(11)][a]
Ru(1)–C(2)	2.179(6)	2.176(6)	2.205(9) [2.199(11)][a]
Ru(1)–C(3)	2.194(6)	2.202(6)	2.193(9) [2.161(9)][a]
Ru(1)–C(4)	2.175(6)	2.126(6)	2.205(9) [2.180(9)][a]
Ru(1)–C(5)	2.212(5)	2.167(7)	2.154(9) [2.163(10)][a]
Ru(1)–C(6)	2.192(6)	2.142(6)	2.177(10) [2.158(11)][a]
C(1)–C(2)	1.409(9)	1.350(12)	1.323(15) [1.397(19)][a]
C(2)–C(3)	1.415(8)	1.360(12)	1.429(16) [1.301(18)][a]
C(3)–C(4)	1.416(8)	1.394(13)	1.418(15) [1.307(16)][a]
C(4)–C(5)	1.429(8)	1.381(13)	1.392(15) [1.485(17)][a]
C(5)–C(6)	1.402(9)	1.337(13)	1.393(15) [1.375(17)][a]
C(1)–C(6)	1.417(9)	1.381(13)	1.387(16) [1.362(19)][a]
N(1)–Ru(1)–O(1)	83.40(17)	87.73(14)	83.4(2) [82.6(2)][a]
N(1)–Ru(1)–N(2)	83.46(18)	78.04(14)	80.35(19) [80.2(2)][a]
N(2)–Ru(1)–O(1)	89.65(16)	87.10(14)	83.32(15) [82.6(2)][a]

[a] The data are for two molecules.

Table 3
Summary of relevant bond distances (Å) in [(η^6-C_6H_6)Ru(L^1-O)][PF_6] (**1**), [(η^6-C_6H_6)Ru(L^3-O)][PF_6] (**3**), and [(η^6-C_6H_6)Ru(L^4-O)][BPh_4] · 1/2CH_3OH · H_2O (**4b** · 1/2CH_3OH · H_2O)

	1	**3**	**4b** · 1/2CH_3OH · H_2O[a]
Av Ru–C	2.1911(6)	2.165(6)	2.186(9) [2.172(10)]
Ru–C_6H_6 (centroid)	1.674	1.680	1.687 [1.686]
Av C–C	1.4146(9)	1.367(13)	1.390(15) [1.372(17)]
Ru–$N_{(py)}$	2.098(5)	2.104(4)	–
Ru–$NMe_{(amine)}$	2.170(5)	2.203(4)	2.141(6) [2.147(6)]
Ru–$NMe_{2(amine)}$	–	–	2.1408(8) [2.1443(12)]
Ru–$O_{(phenolate)}$	2.096(4)	2.054(3)	2.041(5) [2.040(5)]

[a] The data are for two molecules.

of methyl group(s) in **1** and **4b** · 1/2CH_3OH · H_2O than that of benzyl group in **3**. (iv) Within the present group of complexes the phenolate oxygen provides strongest binding to Ru^{II} and the N(amine) provides least effective binding. The Ru–N(py) bond in **1** and **3** is stronger than that of Ru–N(amine) bond and weaker than that of Ru–O(phenolate) bond. As O(phenolate) carries a negative charge it forms strong σ-bond with Ru(II) ion. Pyridine being a π-acceptor binds more effectively than the σ-donating alkylamine (Table 3). (v) In these compounds the distortion at the coordinated benzene ligand is present, with respect to the Ru–C bond distances. In **1** the longest Ru–C bond of 2.212(5) Å [the other Ru–C bonds are between 2.175(6) and 2.195(6) Å] is *trans* to pyridine N atom and the shortest Ru–C bond of 2.175(6) Å is *trans* to phenolate O atom of L^1-O^-. Thus in **1** the extent of *trans* influence follows the order: pyridine > amine > phenolate. In **3** the longest Ru–C bond of 2.202(6) Å [the other Ru–C bonds are between 2.142(6) and 2.180(4) Å] is *trans* to phenolate

O atom and the shorter Ru–C bond of 2.167(7) Å is *trans* to amine N atom of L^3-O^-. Thus in **3** the extent of *trans* influence follows the order: phenolate > pyridine > amine. In **4b** · $1/2CH_3OH \cdot H_2O$ the longest Ru–C bond of 2.205(11) Å [2.199(11) Å] [the other Ru–C bonds are between 2.193(9) Å {2.189(9) Å} and 2.154(9) Å {2.158(11)} Å] is *trans* to phenolate O atom of L^4-O^- and the shorter Ru–C bond of 2.177(10) Å {2.158(11)} Å] is *trans* to NMe_2 amine nitrogen of L^4-O^-. Thus in **4b** · $1/2CH_3OH \cdot H_2O$ the extent of *trans* influence follows the order: phenolate > amine (NMe) > amine (NMe_2). This trend could be rationalized if we take into account the fact that between π-acceptor and σ-donor ligands, in general former ligands have greater *trans* influence than the latter ligands. Moreover, among the σ-donating ligands greater the σ-donor strength larger the *trans* influence. The greater *trans* influence of pyridine in **1** is thus understandable. The O(phenolate) group carrying a negative charge is a better σ-donor, thus its greater *trans* influence than amine N in **1** and **4b** · $1/2CH_3OH \cdot H_2O$ is also understandable. But in **3** the *trans* influence of phenolate O atom is greater than the pyridine N atom. It might be due to the very strong binding by phenolate oxygen in **3** because of the presence of two electron releasing *tert*-butyl groups at the ortho and para position of the phenolate ring in L^3OH (vide supra). In essence, for **1**, **3**, and **4b** · $1/2CH_3OH \cdot H_2O$ the observed trend in Ru–C, Ru–N(py), Ru–N(amine), and Ru–O(phenolate) distances (Table 2), reflecting mutual *trans* influence, is a consequence of interplay between steric and electronic factors associated with the coordinating ability of tridentate ligands L^1-O^-, L^3-O^-, and L^4-O^- in a closely similar metal coordination environment.

The slightly shorter Ru–C_6H_6 centroid distance (Table 3) in **1** (1.674 Å) than that in **3** (1.680 Å) may be attributed to the temperature difference at which the data of the complexes were collected. Between **3** and **4b** · $1/2CH_3OH \cdot H_2O$, the Ru–C_6H_6 centroid distance in **3** (1.680 Å) is less than that in **4b** · $1/2CH_3OH \cdot H_2O$ [1.687 Å {1.686 Å}]. So, the phenolate-based ligands L^1-O^- present in **1** and L^3-O^- present in **3** provide more relative strength to $\{(\eta^6\text{-}C_6H_6)Ru\}^{2+}$ unit than that by L^4-O^- in **4b** · $1/2CH_3OH \cdot H_2O$.

Average Ru–C distances in **1**, **3**, and **4b** · $1/2CH_3OH \cdot H_2O$ (Table 3) are comparable to that reported in similar three-legged piano-stool complexes including $\{(\eta^6\text{-}C_6H_6)RuCl\}^+$ moiety [4,5]. The Ru–N(py) and Ru–N(amine) bond lengths observed in **1** and **3** compare well with the values found in similar three-legged piano-stool complexes with N-donor ligands [4,5]. The Ru–O distances are comparable to that reported in the literature for half-sandwich complexes with phenolate ligands [6].

Notably, due to coordination by the ligands the Ru center assumes a chiral center and in turn the central amine nitrogen also becomes chiral. Therefore, the compounds can be obtained as two diastereomeric pairs of isomers, i.e. SS/RR and SR/RS [2f,16]. However, the two enantiomers of a diastereomeric pair must be in 1:1 ratio to give rise to a racemic mixture. As the ^1H NMR spectra (see below) exhibit only one set of signals it can be concluded that the reaction is completely diastereoselective. Therefore, an attempt has been made to assign the configurations of diastereomers of the complexes **1**, **3**, and **4b**, by X-ray analysis of single-crystals. It is worth mentioning here that for all the structures presented in this work the space group is centrosymmetric $P\bar{1}$. Therefore, both enantiomers of the isolated diastereomeric pair must be present in the unit cell in 1:1 ratio. Notably, in all the cases, structural analysis reveals the presence of only one diastereomer (**1**: S_{Ru},S_N; **3**: S_{Ru},R_N; **4b**: S_{Ru},R_N) in the asymmetric unit. In case of complex **4b**, there are two molecules in the asymmetric unit having same configuration. However, in each case closer inspection of the contents of the unit cell reveals the presence of both the enantiomers of the isolated diastereomeric pair (**1**: $S_{Ru},S_N/R_{Ru},R_N$; **3**: $S_{Ru},R_N/R_{Ru},S_N$; **4b**: $S_{Ru},R_N/R_{Ru},S_N$) in 1:1 ratio. The configuration of the ruthenium center in the complexes **1**, **3**, and **4b** is *S*, in accordance with the ligand priority sequence [16a] ($\eta^6C_6H_6$) > O(PhO) > N(Py) > N(amine) or ($\eta^6C_6H_6$) > O(PhO) > NMe > NMe_2. While the configuration of the central amine nitrogen center in the complexes **1**, **3**, and **4b** are *S*, *R*, and *R*, respectively, in accordance with the priority order [16b] of the four groups Ru > CH_2PhO > $(CH_2)_2Py$ > CH_3, Ru > CH_2PhO > $(CH_2)_2Py$ > CH_2Ph, and Ru > CH_2PhO > $(CH_2)_2NMe_2$ > CH_3, respectively, for the complexes **1**, **3**, and **4b**.

Unfortunately, the crystal data obtained for the compound **2** could not be refined properly because of the presence of 8 molecules [$Z' = 8$, triclinic crystal system ($P\bar{1}$)] [17] in the asymmetric unit and severe disorder associated with *tert*-butyl carbon atoms. However, all eight molecules have been identified and refined isotropically [Fig. S1 (Supplementary material)] and one of the eight molecules is refined anisotropically [Fig. S2 (Supplementary material)]. Interestingly, all eight molecules present in the asymmetric unit are found to have the same configuration about the Ru(II) center and central amine nitrogen center. However, closer inspection of the contents of the unit cell reveals the presence of both enantiomers of the isolated diastereomeric pair ($R_{Ru},R_N/S_{Ru},S_N$) in 1:1 ratio.The configuration of the ruthenium center and central amine nitrogen center of all the molecules in the complex **2** is *R*, in accordance with the priority sequences ($\eta^6C_6H_6$) > O(PhO) > N(Py) > N(amine) and Ru > CH_2PhO > $(CH_2)_2Py$ > CH_3.

3.3. ^1H NMR spectroscopy

^1H NMR data (in CD_3CN) of **1**–**3**, **4a**, and **4b** along with their assignments are recorded in the Experimental section, supporting their expected "piano-stool" structure [Figs. S3–S7 (Supplementary material)]. The proton resonances were assigned based on available ^1H NMR spectral results for the free ligands L^1-OH, L^2-OH, and L^3-OH (this work), and L^4-OH [10]. For complex **3**, the three methylene spacers were unambiguously assigned by the ^1H NOE experiments. The following comments regarding the spectral data are in

order. (i) The chemical shift values for coordinated benzene in the complexes **1**, **2**, **3**, **4a**, and **4b** are δ 5.80, δ 5.84, δ 5.94, δ 5.65, and δ 5.61, respectively. Maximum upfield shift (δ 5.65 and 5.61) for **4a** and **4b** implies the presence of more electron density on the benzene ring than in other compounds. It is understandable as ligand L^4O^- is providing all three coordination (two alkyl amine N atoms and one phenolate O^- anion) with σ-donor ligands and hence Ru^{II} center is pulling less electron density from benzene ring. Maximum downfield shift (δ 5.94) for **3** implies the presence of least electron density on the benzene ring. Among the compounds with pyridine-containing phenolate ligands (L^1-OH, L^2-OH, and L^3-OH) ligand L^3-O^- is a better π-acceptor due to the formation of five- membered chelate ring. Hence in **3** the Ru^{II} center is withdrawing more electron density from benzene ring than that in other cases. It is clearly reflected in its av Ru–C distance (Table 3), implying poor interaction of C_6H_6 ligand with Ru(II) (*cf.* X-ray structure). (ii) An AB quartet for $–CH_2–$ protons of the ligands confirms the presence of two diastereotopic protons, axial and equatorial. It implies that these protons are not interconverting on the NMR time-scale; otherwise a singlet would have resulted. (iii) The methylene hydrogen atoms of $–CH_2CH_2–$ backbone of the ligands are non-equivalent upon complexation and appeared as four multiplets. Some geminal and vicinal coupling in $–CH_2CH_2–$, make a clearer interpretation difficult. (iv) The two aromatic phenolate hydrogen atoms (H3 and H5) of L^2-O^-, L^3-O^-, and L^4-O^- in **2**, **3**, **4a**, and **4b** split on complexation and resulted in two doublets. The formation of rigid structure on complexation supports the clearer visualization of aromatic protons in all the complexes.

The only one set of ^{1}H NMR signals for the complexes **1**–**4a**, and **4b** suggest to believe that the complex formation is diastereoselective. So, to ascertain the configuration of diastereomer present in solution for complexes **1**–**4a**, and **4b**, ^{1}H NOE experiments were carried out. No NOEs were observed between the methylene spacer of phenolate group and ethylene spacer of pyridine in complexes **1**, **2**, and **4b**. This clearly suggests that methylene and ethylene spacers are far away from each other in these complexes. However, for compound **3** several NOEs were observed between the methylene protons [Fig. S5 (Supplementary material)]. The irradiation of the H_a and H_b ($–CH_2–$ of benzyl) protons induces NOE enhancement of the $H_{b'}$ ($–CH_2–$ of PhO) and $H_{b''}$ ($–CH_2–$ of Py) protons and *vice versa*, respectively and the irradiation of $H_{a'}$ ($–CH_2–$ of PhO) induces NOE enhancement of the $H_{a''}$ ($–CH_2–$ of Py) proton and *vice versa*. The NOE results for compound **3** clearly indicate that the diastereomeric pair present in solution is in agreement with that obtained (S_{Ru},R_N/R_{Ru},S_N) from X-ray analysis (single crystals of compound **3**). The ^{1}H NMR spectral features of the samples of **1**–**3**, and **4b** (crushed single-crystals) are identical with those obtained from the bulk powdered samples of the corresponding complexes, showing the presence of a single diastereomeric pair in solution.

In essence, the ^{1}H NMR results of **1**–**3**, and **4b** clearly indicate that the solid state structures (vide supra) are retained in solution.

3.4. Non-covalent interactions

A closer inspection of the crystal packing diagrams of **1** and **3** reveals that these organometallic molecules are engaged in secondary interactions (see below). Relevant bond distances, bond angles, and symmetry are summarized in Table 4. The C–H···O hydrogen-bonding parameters observed in this work [2.466–2.598 Å and 117.1–145.2° (**1**); 2.658 Å and 171.5°(**3**)] are in good agreement with literature tabulations (C–H···O: 2.045–2.399 Å and 90.7–176.7°) [18], literature precedents [19] including our own findings [20]. These can be classified as intermediate contacts (2.439–2.598 Å) which are appreciably shorter than the sum of the van der Waals radii for the H and the neutral O atoms (2.72 Å) [19b].

3.4.1. $[(\eta^6\text{-}C_6H_6)Ru(L^1\text{-}O)][PF_6]$ (**1**) and $[(\eta^6\text{-}C_6H_6)\text{-}Ru(L^3\text{-}O)][PF_6]$ (**3**)

The analysis of crystal structures of **1** and **3** reveals that these half-sandwich organometallic molecules are engaged in secondary interactions in the form of hydrogen bonds leading to the formation of supramolecular arrays [20]. In both the structures dimeric units are formed *via* intermolecular C–H···O hydrogen-bonding interactions. In **1** the phenolate oxygen is not participating in hydrogen bonding but the oxygen atoms of nitro group present at *para* position on phenolate ring of L^1-O^- are involved in bifurcated hydrogen-bonding. This is an example of self-complementary hydrogen-bonding interactions. The bifurcated C–H···O hydrogen-bonding interactions involving H(14B) of *N*-methyl and H(6) of Ru-coordinated benzene with O(3) of nitro group leads to the formation of dimeric motif [Fig. 2a]. These dimeric units in **1** are involved in another bifurcated self-complementary C–H···O hydrogen-bonding interactions involving H(1) and H(2) of Ru-coordinated benzene with O(2) of nitro group leading to the formation of one-dimensional hydrogen-bonded chain (Fig. 3).

Table 4
Hydrogen-bonding (C–H···O) parameters for $[(\eta^6\text{-}C_6H_6)Ru(L^1\text{-}O)]^+$ in **1** and $[(\eta^6\text{-}C_6H_6)Ru(L^3\text{-}O)]^+$ in **3**

D–H···*A*	H···*A* (Å)	*D*···*A* (Å)	*D*–H···*A*
$[(\eta^6\text{-}C_6H_6)Ru(L^1\text{-}O)]^+$ unit in **1**			
C1–H1···O2	2.598[i]	3.2487(4)[i]	117.8°[ii]
C2–H2···O2	2.466[i]	3.1929(3)[i]	123.3°[ii]
C6–H6···O3	2.496[iii]	3.1420(3)[iii]	117.1°[iii]
C14–H14B···O3	2.481[iii]	3.4273(4)[iii]	145.2°[iii]
$[(\eta^6\text{-}C_6H_6)Ru(L^3\text{-}O)]^+$ unit in **3**			
C25–H25A···O1	2.658[iv]	3.6988(4)[iv]	171.5°[iv]

[i] $1+x, 1+y, z$.
[ii] $-1+x, 1+y, z$.
[iii] $2-x, 1-y, 1-z$.
[iv] $2-x, -y, -z$.

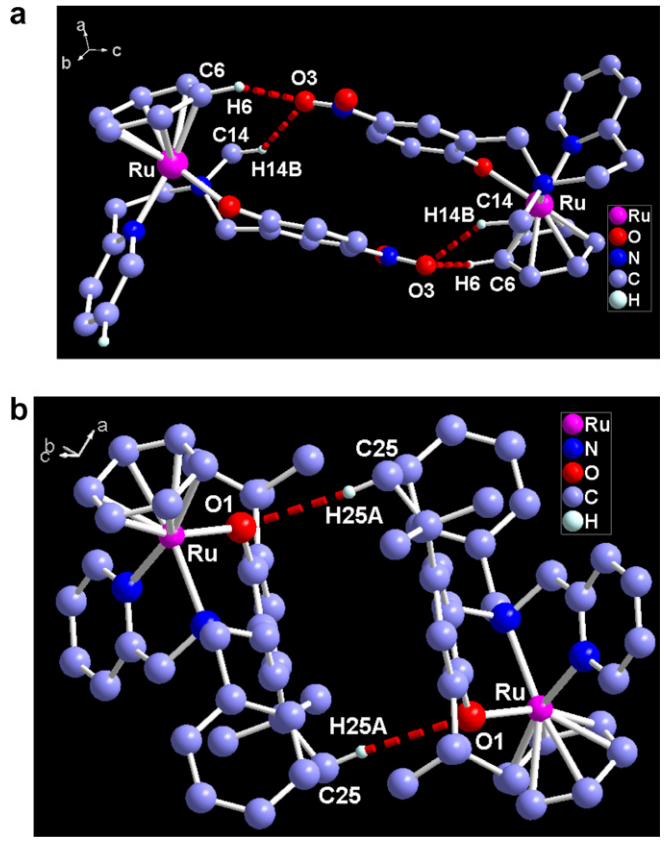

Fig. 2. View of the formation of dimer through C–H···O hydrogen bonding in (a) $[(\eta^6\text{-}C_6H_6)Ru(L^1\text{-}O)]^+$ unit in **1** and (b) $[(\eta^6\text{-}C_6H_6)Ru(L^3\text{-}O)]^+$ unit in **3**. All the hydrogen atoms except those involved in hydrogen bonding have been omitted for clarity.

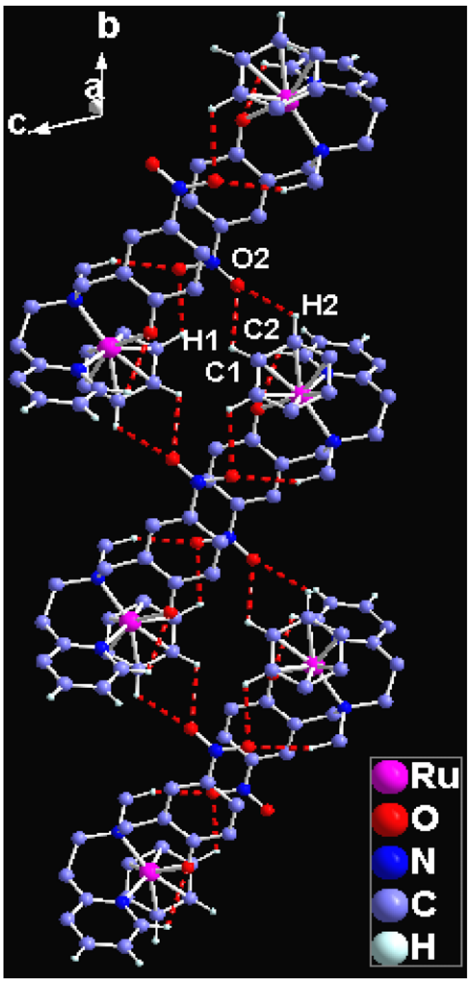

Fig. 3. View of the formation of the bimolecular 1-D chain through C–H···O hydrogen bonding in $[(\eta^6\text{-}C_6H_6)Ru(L^1\text{-}O)]^+$ unit in **1**. All the hydrogen atoms except those involved in hydrogen bonding have been omitted for clarity.

In **3** the C–H···O interaction involving C–H(H25A) of *tert*-butyl group present at the *para* position of phenolate ring and Ru-coordinated phenolate O(1) leads to the formation of dimeric motifs, *via* self-complementary hydrogen-bonding interactions (Fig. 2b).

3.5. Electrochemical studies

From the standpoint of investigating the potential of the chosen ligands (Scheme 1) to generate phenoxyl radical species, cyclic voltammetric (CV) experiments on the present compounds were performed at 298 K in CH_3CN containing 0.1 M TBAP as the supporting electrolyte. It was revealed that complex **1** is redox-inactive. As expected, due to the presence 2,4-di-*tert*-butylphenolate groups, compounds **2**, **3**, and **4a** display a reversible one-electron oxidative process at $E_{1/2}$ values (V vs. SCE) of 0.74, 0.82, and 0.78, respectively. The redox processes correspond to the reversible formation of phenoxyl radical species $[\mathbf{2}]^{2+\cdot}$, $[\mathbf{3}]^{2+\cdot}$, and $[\mathbf{4a}]^{2+\cdot}$, respectively. The one-electron nature of redox processes are revealed by constant potential (V vs. SCE) electrolysis [0.94, n (the number of electron passed per molecule) = 0.97; 1.0, $n = 1.12$; 0.97, $n = 0.94$ for **2**, **3**, and **4a**, respectively]. The electrogenerated blue ($[\mathbf{2}]^{2+\cdot}$ and $[\mathbf{3}]^{2+\cdot}$) and greenish blue ($[\mathbf{4a}]^{2+\cdot}$) solutions are stable enough for their CV, absorption, and EPR spectra to be recorded. It is, therefore, logical to assume that there is no gross structural change during redox process. One-electron oxidized complexes $[\mathbf{2}]^{2+\cdot}$, $[\mathbf{3}]^{2+\cdot}$, and $[\mathbf{4a}]^{2+\cdot}$ display in CH_3CN solution reversible ($\Delta E_p = 70$ mV for $[\mathbf{2}]^{2+\cdot}$ and $[\mathbf{3}]^{2+\cdot}$; 80 mV for $[\mathbf{4a}]^{2+\cdot}$) CV responses at 0.75, 0.82, and 0.77 V vs. SCE, respectively (Figs. S8–S10, Supplementary material).

It is worth comparing the redox behavior of complexes **2**, **3**, and **4a** with that of **1**. In the latter case no oxidative response could be seen. This finding is understandable given the presence of two electron-releasing *tert*-butyl groups at *o*- and *p*-positions of phenolate rings in the ligands $L^2\text{-}O^-$, $L^3\text{-}O^-$, and $L^4\text{-}O^-$ rendering the phenolate rings electron-rich and hence facilitating the removal of an electron, which in turn stabilizes phenoxyl radical formed due to one-electron oxidative processes. The bulky *tert*-butyl groups provide hydrophobic environment which helps in stabilization of the generated radical species. It is also worth noting here that the complexes **2**, **3**, and **4a** all

having identical phenolate moiety but still the observed $E_{1/2}$ values are different. The present trend in $E_{1/2}$ values of complexes **2**, **3**, and **4a** can be rationalized by considering the coordinating properties of the two N-donor sites provided by the appended arm to the phenolate moiety, which differ in ligands L^2-O^-, L^3-O^-, and L^4-O^- in complexes **2**, **3**, and **4a**, respectively. Apart from benzene and one phenolate oxygen coordination in **2** and **3** both the fifth and sixth coordinations are provided by one pyridine nitrogen and one alkylamine nitrogen. But in **2** the pyridine nitrogen and alkylamine nitrogen is forming a six-membered chelate ring and in **3** it is forming a five-membered chelate ring. It is well-established that a five-membered chelate-ring forming ligand provide better binding to a metal ion than a six-membered chelate-ring forming ligand. Pyridine is a π-accepting ligand and it is expected to act as a better π-acceptor, when present as a part of a five-membered chelate ring. Therefore, in **3** pyridine is withdrawing more electron density from Ru^{II} center and as a consequence of which Ru^{II} is withdrawing more electron density from phenolate oxygen and benzene (*cf.* ^1H NMR and X-ray structure). This in turn makes the phenolate oxygen comparatively poorer in electron density in **3** than in **2**. Thus, between **2** and **3** it is understandable why the $E_{1/2}$ value for **3** (0.82 V vs. SCE) is more anodic than **2** (0.74 V vs. SCE). Notably, in **4a** two coordinations are provided by σ-donating alkylamine nitrogens and they are involved in the formation of a five-membered chelate ring. So why the $E_{1/2}$ value for **4a** (0.78 V vs. SCE) is lower than that of **3** is understandable. The higher $E_{1/2}$ value for **4a** than that of **2** (0.74 V vs. SCE), may be attributed to better binding ability of pyridine nitrogen, due to π-accepting property, than the alkylamine nitrogen Fig. 4.

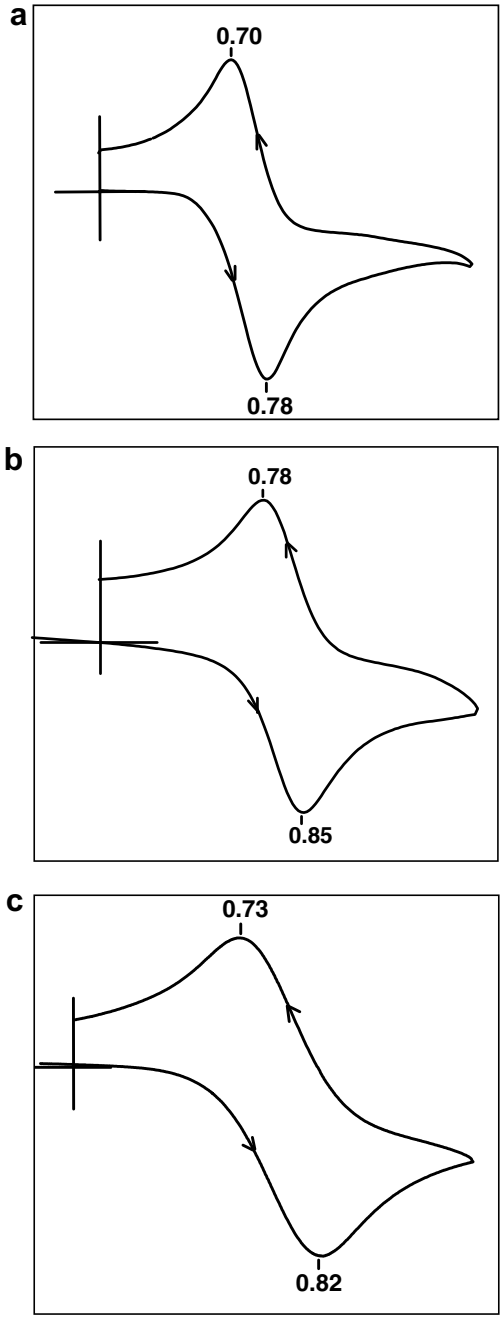

Fig. 4. Cyclic voltammogram (scan rate: 100 mV s^{-1}) of ~1.0×10^{-3} mol dm^{-3} CH_3CN (~0.1 mol dm^{-3} in TBAP) solution of (a) $[(\eta^6\text{-}C_6H_6)Ru(L^2\text{-}O)][PF_6]$ (**2**), (b) $[(\eta^6\text{-}C_6H_6)Ru(L^3\text{-}O)][PF_6]$ (**3**), and (c) $[(\eta^6\text{-}C_6H_6)Ru(L^4\text{-}O)][PF_6]$ (**4a**) at a Pt working electrode. Indicated potentials (in V) are vs. SCE.

3.6. Stability of phenoxyl radical coordinated Ru^{II} species

We subjected the one-electron oxidized solutions of phenoxyl radical coordinated Ru^{II} species to UV–Vis and EPR spectroscopy. Solutions of **2**, **3**, and **4a** in CH_3CN are orange; however, the one-electron oxidized counterparts are blue to greenish blue in color. The electronic spectra of electrochemically generated solutions of $[\mathbf{2}]^{2+\cdot}$ [Fig. 5 (dotted line)], $[\mathbf{3}]^{2+\cdot}$ and $[\mathbf{4}]^{2+\cdot}$ (Figs. S11 and S12, Supplementary material) show two characteristic absorptions: 390 nm ($\epsilon \sim 3100$ dm^3 mol^{-1} cm^{-1}) and 680 nm

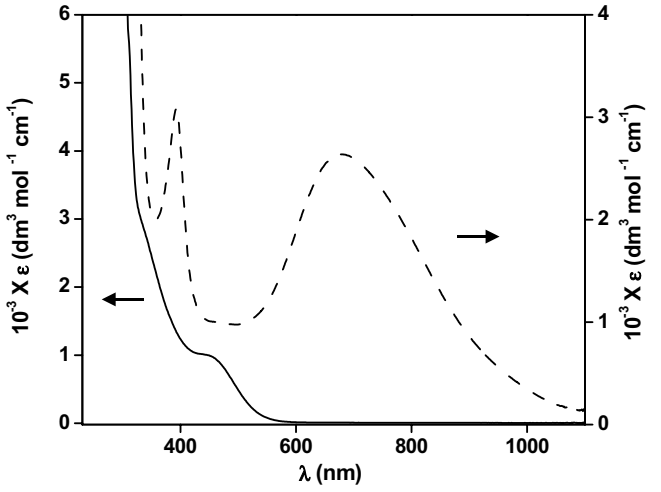

Fig. 5. UV–Vis spectra (in CH_3CN) of $[(\eta^6\text{-}C_6H_6)Ru(L^2\text{-}O)][PF_6]$ (**2**) (—) and $[(\eta^6\text{-}C_6H_6)Ru(L^2\text{-}O)]^{2+\cdot}$ $[\mathbf{2}]^{2+\cdot}$ (– – –), generated in solution by coulometric oxidation of **2**.

($\epsilon \sim 2650\ dm^3\ mol^{-1}\ cm^{-1}$) for $[\mathbf{2}]^{2+\cdot}$; 395 nm ($\epsilon \sim 2200\ dm^3\ mol^{-1}\ cm^{-1}$) and 850 nm ($\epsilon \sim 1550\ dm^3\ mol^{-1}\ cm^{-1}$) for $[\mathbf{3}]^{2+\cdot}$; 395 nm ($\epsilon \sim 3200\ dm^3\ mol^{-1}\ cm^{-1}$) and 720 nm ($\epsilon \sim 3250\ dm^3\ mol^{-1}\ cm^{-1}$) for $[\mathbf{4a}]^{2+\cdot}$. Similar absorptions have previously been observed for phenoxyl radicals and are attributed to π–π^* transitions [9a]. All the three phenoxyl radical complexes are moderately stable in air and at ambient temperature, but gradually decompose *via* first-order kinetics. Complex $[\mathbf{4a}]^{2+\cdot}$ is most stable with $k_{decay} = 4.99 \times 10^{-3}\ min^{-1}$ followed by $[\mathbf{2}]^{2+\cdot}$ with $k_{decay} = 8.15 \times 10^{-3}\ min^{-1}$ and $[\mathbf{3}]^{2+\cdot}$ with $k_{decay} = 4.33 \times 10^{-2}\ min^{-1}$. A plot of decay for $[\mathbf{2}]^{2+\cdot}$ is shown in Fig. 6 (inset) and for $[\mathbf{3}]^{2+\cdot}$ and $[\mathbf{4a}]^{2+\cdot}$ in Figs. S13 and S14 (Supporting Information). Kinetic studies reveal that the phenoxyl radical coordinated to Ru(II) complexes having "piano-stool geometry" is more stable than the reported Zn^{II} and Cu^{II} coordinated similar phenoxyl radical species [9d]. An interesting spectral change was observed during the gradual decomposition of $[\mathbf{2}]^{2+\cdot}$ and $[\mathbf{3}]^{2+\cdot}$. An intense band around 1000 nm appears. So far we could not identify the decomposed products. Efforts are underway to isolate and establish the identity of such end-products.

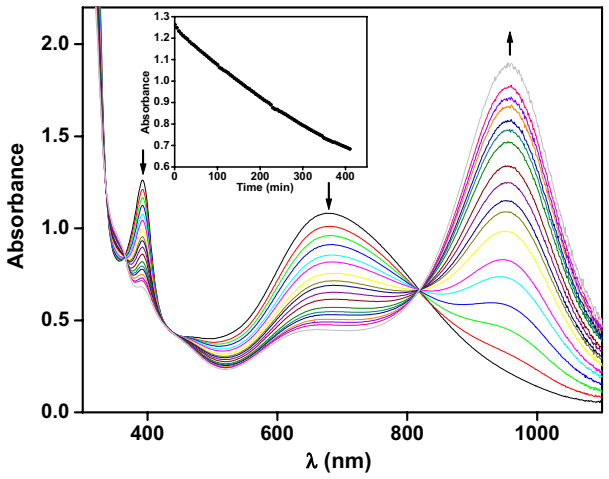

Fig. 6. Spectral change due to the formation and decomposition of the phenoxyl radical complex $[(\eta^6\text{-}C_6H_6)Ru(L^2\text{-}O)]^{2+\cdot}$ $[\mathbf{2}]^{2+\cdot}$ in CH_3CN (0.1 mol dm^{-3} TBAP) at 298 K. Inset: first-order plot of decay.

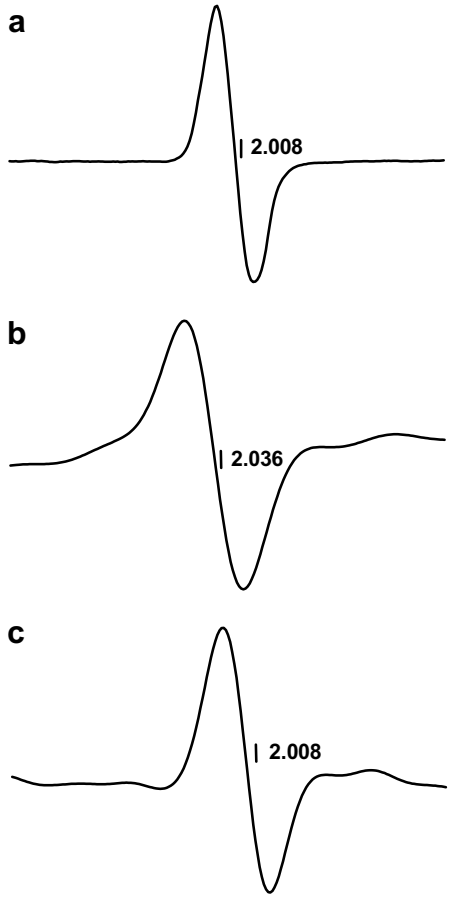

Fig. 7. EPR spectra in a mixture of CH_3CN and toluene (2:1; v/v) of (a) $[(\eta^6\text{-}C_6H_6)Ru(L^2\text{-}O)]^{2+\cdot}$ $[\mathbf{2}]^{2+\cdot}$ (b) $[(\eta^6\text{-}C_6H_6)Ru(L^3\text{-}O)]^{2+\cdot}$ $[\mathbf{3}]^{2+\cdot}$ and (c) $[(\eta^6\text{-}C_6H_6)Ru(L^4\text{-}O)]^{2+\cdot}$ $[\mathbf{4a}]^{2+\cdot}$ [coulometrically generated in CH_3CN].

In line with expectation the X-band EPR spectra in CH_3CN/toluene at 298 K of the electrochemically oxidized phenoxyl radical forms of **2**, **3**, and **4a** exhibit isotropic (g_{iso}) signals at 2.008, 2.036, and 2.008, respectively (Fig. 7).

4. Conclusions

Despite a few examples of structurally characterized mononuclear three-legged half-sandwich complexes of type $[\{(\eta^6\text{-}C_6H_6)Ru(L)\}^+$ [L = mononegative salicylaldehyde-based Schiff base ligand (only one example with reduced Schiff base ligand)], no report is available in the literature on systematic studies of similar complexes with use of pyridylalkylamine/alkylamine–phenolate-based tridentate non-Schiff base ligands. In this work we have provided four such examples. Notably, due to coordination by the ligands the Ru center assumes a chiral center and in turn the central amine nitrogen also becomes chiral. The ^1H NMR spectra exhibit only one set of signals; thus the reaction is completely diastereoselective. Interestingly, we were able to discover that two such complexes are involved in non-covalent interactions (C–H···O) in the solid state. Notably, out of four ligands chosen in this work three carry sites suitable for one-electron ligand-based oxidation, leading to generation of Ru^{II}-coordinated phenoxyl radical-based ligands. Such species have been characterized by cyclic voltammetry, UV–Vis, and EPR spectroscopy. Stability of these species has been followed by absorption spectroscopy. The present study thus provides further information on complexes of type $[\{(\eta^6\text{-}C_6H_6)Ru(L)\}^{2+\cdot}$, which are one-electron oxidized counterparts of $[\{(\eta^6\text{-}C_6H_6)Ru(L)\}^+$.

Acknowledgements

This work is supported by Grants from the Department of Science and Technology, Government of India and the Council of Scientific and Industrial Research, New Delhi.

HM gratefully acknowledges University Grants Commission (UGC), New Delhi for a Junior Research Fellowship. We thank Atasi Mukherjee for the synthesis of 2,4-di-*tert*-butyl-6-(chloromethyl)phenol fragment. We thank Himanshu Arora for kinetic study of the complexes. We gratefully acknowledge Prof. Y.D. Vankar of our Department for his valuable suggestion in determining the configuration of the compounds. R.M. gratefully acknowledges the award of a joint collaborative Grant with Prof. Siegfried Schindler funded by the Volkswagen Foundation, Germany and the donation of a HP 8453 diode-array spectrophotometer. Comments of the reviewers at the revision stage are highly appreciated.

Appendix A. Supplementary material

CCDC 631899, 631900, and 632188 contain the supplementary crystallographic data for **1**, **3**, and **4b** · $1/2CH_3OH \cdot H_2O$. These data can be obtained free of charge via http://www.ccdc.cam.ac.uk/conts/retrieving.html, or from the Cambridge Crystallographic Data Centre, 12 Union Road, Cambridge CB2 1EZ, UK; fax: (+44) 1223-336-033; or e-mail: deposit@ccdc.cam.ac.uk. Supplementary data associated with this article can be found, in the online version, at doi:10.1016/j.jorganchem.2007.03.041.

References

[1] (a) H. Le Bozec, D. Touchard, P.H. Dixneuf, Adv. Organomet. Chem. 29 (1989) 163–247;
(b) M.A. Bennett, Coord. Chem. Rev. 166 (1997) 225–254.
[2] (a) R. Noyori, S. Hashiguchi, Acc. Chem. Res. 30 (1997) 97–102;;
(b) T. Naota, H. Takaya, S.-I. Murahashi, Chem. Rev. 98 (1998) 2599–2660;
(c) M.J. Palmer, M. Wills, Tetrahedron: Asym. 10 (1999) 2045–2061;
(d) R.K. Rath, M. Nethaji, A.R. Chakravarty, Polyhedron 20 (2001) 2735–2739;
(e) D. Carmona, M.P. Lamata, L.A. Oro, Eur. J. Inorg. Chem. (2002) 2239–2251;
(f) A.J. Davenport, D.L. Davies, J. Fawcett, D.R. Russell, J. Chem. Soc., Dalton Trans. (2004) 1481–1492;
(g) D. Carmona, M.P. Lamata, F. Viguri, J. Ferrer, N. García, F.J. Lahoz, M.L. Martin, L.A. Oro, Eur. J. Inorg. Chem. (2006) 3155–3166.
[3] A. Habtemariam, M. Melchart, R. Fernández, S. Parsons, I.D.H. Oswald, A. Parkin, F.P.A. Fabbiani, J.E. Davidson, A. Dawson, R.E. Aird, D.I. Jodrell, P.J. Sadler, J. Med. Chem. 49 (2006) 6858–6868, and references therein.
[4] Z. Shirin, R. Mukherjee, J.F. Richardson, R.M. Buchanan, J. Chem. Soc., Dalton Trans. (1994) 465–469.
[5] H. Mishra, R. Mukherjee, J. Organomet. Chem. 691 (2006) 3545–3555.
[6] (a) S.K. Mandal, A.R. Chakravarty, J. Organomet. Chem. 417 (1991) C59–C62;
(b) S.K. Mandal, A.R. Chakravarty, J. Chem. Soc., Dalton Trans. (1992) 1627–1633;
(c) S.K. Mandal, A.R. Chakravarty, Inorg. Chem. 32 (1993) 3851–3854;
(d) S. Roy, C. Sudha, A.R. Chakravarty, Indian J. Chem. 37A (1998) 1045–1051;
(e) S. Roy, R.K. Rath, C. Sudha, A.R. Chakravarty, Indian J. Chem. 39A (2000) 838–842;
(f) H. Brunner, T. Zwack, M. Zabel, Organometallics 22 (2003) 1741–1750.
[7] (a) R.I. Haines, D.R. Hutchings, T.M. McCormack, J. Inorg. Biochem. 85 (2001) 1–7;
(b) A.D. Ryabov, V.S. Sukharev, L. Alexandrova, R. Le Lagadec, M. Pfeffer, Inorg. Chem. 40 (2001) 6529–6532;
(c) R. Bhalla, C.J. Boxwell, S.B. Duckett, P.J. Dyson, D.G. Humphrey, J.W. Steed, P. Suman, Organometallics 21 (2002) 924–928;
(d) H. Jude, J.A.K. Bauer, W.B. Connick, J. Am. Chem. Soc. 125 (2003) 3446–3447;
(e) A. Singh, M. Chandra, A.N. Sahay, D.S. Pandey, K.K. Pandey, S.M. Mobin, M.C. Puerta, P. Valerga, J. Organomet. Chem. 689 (2004) 1821–1834;
(f) R. Le Lagadec, L. Rubio, L. Alexandrova, R.A. Toscano, E.V. Ivanova, R. Meškis, V. Laurinavičius, M. Pfeffer, A.D. Ryabov, J. Organomet. Chem. 689 (2004) 4820–4832;
(g) M. Nomura, M. Fujii, K. Fukuda, T. Sugiyama, Y. Yokoyama, M. Kajitani, J. Organomet. Chem. 690 (2005) 1627–1637;
(h) P. Štěpnička, J. Ludvík, J. Canivet, G. Süss-Fink, Inorg. Chim. Acta 359 (2006) 2369–2374;
(i) R. Poli, Angew. Chem., Int. Ed. 45 (2006) 5058–5070;
(j) L.-H. Bi, E.V. Chubarova, N.H. Nsouli, M.H. Dickman, U. Kortz, B. Keita, L. Nadjo, Inorg. Chem. 45 (2006) 8575–8583.
[8] (a) A.K. Patra, R. Mukherjee, Inorg. Chem. 38 (1999) 1388–1393;
(b) A.K. Patra, M. Ray, R. Mukherjee, Inorg. Chem. 39 (2000) 652–657;
(c) A.K. Singh, V. Balamurugan, R. Mukherjee, Inorg. Chem. 42 (2003) 6497–6502, and references therein.
[9] (a) A. Sokolowski, J. Müller, T. Weyhermüller, R. Schnepf, P. Hildebrandt, K. Hildenbrand, E. Bothe, K. Wieghardt, J. Am. Chem. Soc. 119 (1997) 8889–8900;
(b) J.A. Halfen, B.A. Jazdzewski, S. Mahapatra, L.M. Berreau, E.C. Wilkinson, L. Que Jr., W.B. Tolman, J. Am. Chem. Soc. 119 (1997) 8217–8227;
(c) P. Chaudhuri, M. Hess, J. Muller, K. Hildenbrand, E. Bill, T. Weyhermu- ller, K. Wieghardt, J. Am. Chem. Soc. 121 (1999) 9599–9610;
(d) M. Taki, H. Kumei, S. Itoh, S. Fukuzumi, J. Inorg. Biochem. 78 (2000) 1–5;
(e) M. Taki, H. Kumei, S. Nagatomo, T. Kitagawa, S. Itoh, S. Fukuzumi, Inorg. Chim. Acta 300 (2000) 622–632;
(f) A. dos Anjos, A.J. Bortoluzzi, Renata E.H.M.B. Osorio, R.A. Peralta, G.R. Friedermann, A.S. Mangrich, A. Neves, Inorg. Chem. Commun. 8 (2005) 249–253;
(g) A. dos Anjos, A.J. Bortoluzzi, B. Szpoganicz, M.S.B. Caro, G.R. Friedermann, A.S. Mangrich, Ademir Neves, Inorg. Chim. Acta 358 (2005) 3106–3114;
(h) M. Lanznaster, H.P. Hratchiran, M.J. Heeg, L.M. Hryhorczuk, B.R. MacGarvey, H.B. Schlegel, C.N. Verani, Inorg. Chem. 45 (2006) 955–957;
(i) R.A. Peralta, A. Neves, A.J. Bortoluzzi, A. dos Anjos, F.R. Xavier, B. Szpoganicz, H. Terenzi, M.C.B. de Oliveira, E. Casetallano, G.R. Friedermann, A.S. Mangrich, M.A. Novak, J. Inorg. Biochem. 100 (2006) 992–1004.
[10] (a) C.K. Williams, L.E. Breyfogle, S.K. Choi, W. Nam, V.G. Young Jr., M.A. Hillmyer, W.B. Tolman, J. Am. Chem. Soc. 125 (2003) 11350–11359;
(b) A.S. Mangrich, M.A. Novak, J. Inorg. Biochem. 100 (2006) 992–1004.
[11] R.A. Zelonka, M.C. Baird, Can. J. Chem. 50 (1972) 3063–3072.
[12] L.J. Farrugia, WinGX ver 1.64, An integrated systems of windows programs for the solution, refinement and analysis of single-crystal X-ray diffraction data, Department of Chemistry, University of Glasgow, 2003.
[13] DIAMOND ver 2.1c, Crystal Impact GbR, Bonn, Germany, 1999.
[14] T. Steiner, Angew. Chem., Int. Ed. 41 (2002) 48–76.
[15] W.J. Geary, Coord. Chem. Rev. 7 (1971) 81–122.

[16] (a) K. Stanley, M.C. Baird, J. Am. Chem. Soc. 97 (1975) 6598–6599;
(b) R.S. Canh, C. Ingold, V. Prelog, Angew. Chem., Int. Ed. Engl. 5 (1966) 385–415.
[17] J.W. Steed, CrystEngCommun 5 (2003) 169–179.
[18] R. Taylor, O. Kennard, J. Am. Chem. Soc. 104 (1982) 5063–5070.
[19] (a) L. Scaccianoce, D. Braga, M.J. Calhorda, F. Grepioni, B.F.G. Johnson, Organometallics 19 (2000) 790–797;
(b) L. Brammer, in: G.R. Desiraju (Ed.), Perspectives in Supramolecular Chemistry – Crystal Design: Structure and Function, vol. 7, Wiley, Chichester, 2003, pp. 1–75.
[20] V. Balamurugan, M.S. Hundal, R. Mukherjee, Chem. Eur. J. 10 (2004) 1683–1690.